

# Operational implementation of RTTOV-10 in the IFS

Niels Bormann, Alan Geer and Tomas  
Wilhelmsson

Research Department

September 2011

*This paper has not been published and should be regarded as an Internal Report from ECMWF.*

*Permission to quote from it should be obtained from the ECMWF.*



Series: ECMWF Technical Memoranda

A full list of ECMWF Publications can be found on our web site under:

<http://www.ecmwf.int/publications/>

Contact: [library@ecmwf.int](mailto:library@ecmwf.int)

©Copyright 2011

European Centre for Medium-Range Weather Forecasts  
Shinfield Park, Reading, RG2 9AX, England

Literary and scientific copyrights belong to ECMWF and are reserved in all countries. This publication is not to be reprinted or translated in whole or in part without the written permission of the Director-General. Appropriate non-commercial use will normally be granted under the condition that reference is made to ECMWF.

The information within this publication is given in good faith and considered to be true, but ECMWF accepts no liability for error, omission and for loss or damage arising from its use.

## Abstract

This memorandum summarises the evaluation of RTTOV-10 for use in the operational assimilation system at ECMWF. The new features of RTTOV-10 evaluated here are a revised treatment of the top-of-the-atmosphere, and a new sea surface emissivity model for microwave frequencies (FASTEM-4). The new version of RTTOV is evaluated through comparisons of radiative transfer simulations with RTTOV-9, and through an analysis of departure characteristics against observations. The impact on forecasts is also investigated through a series of assimilation experiments.

The use of FASTEM-4 leads to significantly different bias characteristics, primarily for the microwave imager channels used in the ECMWF system. With FASTEM-4, brightness temperature biases against observations are overall within the size of biases between different instruments for imagers, even though biases for some channels on some sensors are degraded compared to using FASTEM-2. The benefits of FASTEM-4 compared to FASTEM-3 are less clear for AMSU-A for which significant biases remain for the window channels.

The changes to the treatment of the top-of-the-atmosphere in RTTOV-10 lead to minor changes to the departure characteristics of channels with some sensitivity to the top of the atmospheric model. Nevertheless, changes are noticeable in the mean temperature analyses above 1 hPa.

The impact of RTTOV-10 on medium-range forecasts is neutral.

## 1 Introduction

This memorandum summarises the evaluation of RTTOV-10 for use in the operational assimilation system at ECMWF. RTTOV is the radiative transfer model used to assimilate radiances at ECMWF (e.g., Saunders et al. 1999), and it is developed and maintained at ECMWF and elsewhere by the NWP SAF, coordinated by the Met. Office. Version 10 is the latest update, released on 27 January 2011, and ECMWF serves as a beta-tester during the final evaluation of the software. RTTOV is a fast radiative transfer model that calculates effective layer optical depths for each channel using regressions derived from line-by-line calculations for layers between fixed pressure levels. Parameterisations to model effects of clouds and rain in the infrared and microwave part of the spectrum are also included.

The main enhancements of RTTOV-10, in terms of direct relevance to the operational use of RTTOV, are an upgrade of the microwave ocean-surface emissivity model to FASTEM-4 (Liu et al. 2011), and the explicit treatment of the top-of-the-atmosphere in the RTTOV code. The software interface has also been revised completely. Other new features are an efficient calculation of principal component scores for AIRS and IASI (Matricardi 2010), a parameterisation of the Zeeman effect for the top-most AMSU-A and several SSMIS channels (Han 2007), as well as support for providing land surface emissivities from an atlas as input to RTTOV for infrared or microwave instruments. RTTOV-10 also includes an improved parameterisation of cloud-overlap assumptions for RTTOV\_SCATT - the configuration of RTTOV used at ECMWF in the all-sky system for microwave imaging instruments. These have been previously evaluated separately at ECMWF (Geer et al. 2009, operational since cycle 35r2). In this memorandum, we describe only the effects of the first two changes, FASTEM-4, and the enhancements at the top-of-the-atmosphere used by RTTOV; the other changes require further developments and are subject of other research efforts.

In the ECMWF system, RTTOV is part of the observation operator for all nadir radiances. Since the implementation of RTTOV-9, the radiative transfer calculations have been performed on the forecast model levels (Bormann et al. 2009), with optical depths provided by RTTOV's regression-based parameterisation of effective layer optical depths. The optical depth calculations are performed on a set of fixed pressure levels, and the input profiles are internally interpolated to these pressure levels using an interpolation scheme that preserves smooth gradients (Rochon et al. 2007). The same scheme is also used to

interpolate the optical depth values to the forecast model levels for the radiative transfer integration. The optical depth parameterisation as well as the choice of surface emissivity models and other parameters are set through coefficient files that can be changed independently of the RTTOV code.

The official RTTOV-10 release also provides a new set of coefficient files based on different or revised spectroscopy and different atmospheric layering (51 or 101 rather than 44 levels). These coefficient files were not available during the beta testing of the RTTOV code, and further work is required to evaluate which of the many coefficient file options is most suitable. This aspect is not covered in the present memorandum, and an update of coefficient files can be performed independently of the RTTOV code. Note that there is a change in the format of the coefficient files between RTTOV-9 and RTTOV-10. Old files used so far in the IFS have been converted to comply with this new format.

## 2 Explicit treatment of the top-of-the-atmosphere

We will first investigate the influence of the changes to the treatment of the top-of-the-atmosphere. This change is not controlled through a switch in the coefficient files and is therefore an integral part of RTTOV-10.

RTTOV-10 explicitly handles the top-of-the-atmosphere used in the line-by-line calculations underlying the optical depth parameterisations. In older versions of RTTOV, this top level (at 0.005 hPa) was implicitly handled in the code, and an isothermal “hidden” layer was assumed above the next RTTOV level located usually at 0.1 hPa for standard 44-level coefficient files. With the move to performing the radiative transfer calculations on forecast model levels with RTTOV-9, a local ECMWF modification of RTTOV relaxed this feature to allow a reasonable estimation of optical depths for forecast model levels above the 0.1 hPa level and to use forecast model temperatures for the source function of the radiative transfer integral above 0.1 hPa (Bormann et al. 2009). An isothermal layer was assumed above the highest forecast model level (at 0.01 hPa). In RTTOV-10, the top-most RTTOV level is properly taken explicitly into account in the standard RTTOV code, and hence treated like any other of the fixed pressure levels. The change is primarily a technical one, correcting a previously scientifically incorrect handling of the top layer in RTTOV-10, but it has noticeable impact on the simulation of some brightness temperatures.

With the change to the top level, the behaviour of the radiative transfer integration has also been changed slightly for the IFS implementation. Now the layer-to-space optical depth is set to zero for the top-most forecast model level, in effect, lowering the top of the atmosphere from RTTOV’s implicit 0.005 hPa top level to the top of the forecast model at 0.01 hPa. An alternative choice would have been to extend the input profile to RTTOV by an extra level at 0.005 hPa, filled, for instance, with data taken from the climatological reference profiles given in the RTTOV coefficient files. This option has in fact been coded up, but it is not used in the tests reported here, as the reference profile values for 0.005 hPa in the coefficient files used here are not considered realistic.

### 2.1 Impact on radiative transfer simulations

As expected, the modification to the treatment of the top-of-the-atmosphere has a rather small impact on the brightness temperatures simulated by RTTOV, and the impact is confined to channels with some sensitivity to the upper stratosphere. To investigate the influence of the changes on the simulated brightness temperatures, we compared brightness temperatures simulated from the same First Guess (FG) profiles

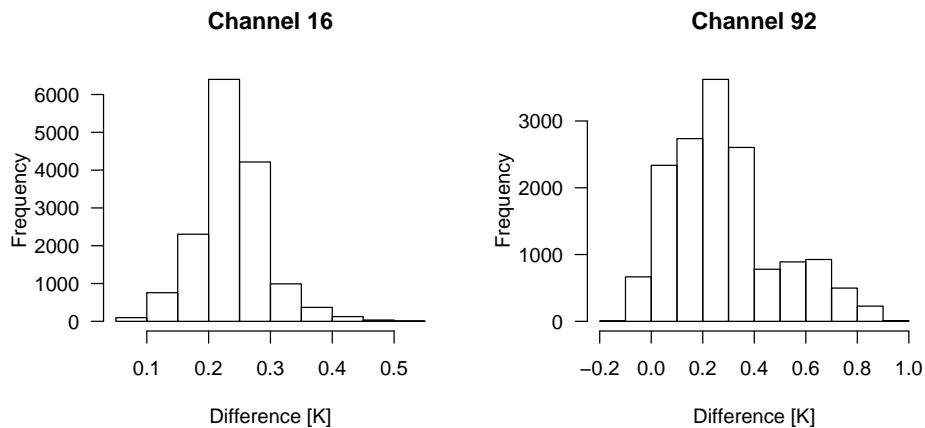


Figure 1: Histogram of differences between FG simulations with RTTOV-10 and RTTOV-9 for two IASI channels (channel 16, peaking at 8 hPa, left, and channel 92, peaking at 2 hPa, right, respectively), based on IASI data from a 12-hour period covering 1 January 2011, 0Z.

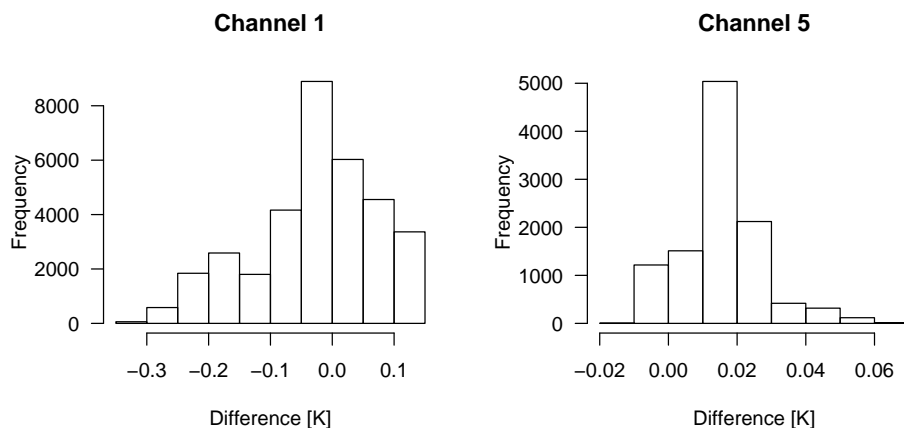


Figure 2: As Fig. 1, but for two HIRS channels (channel 1, sensitive to temperature from 70 to around 1 hPa, left, and channel 5, peaking around 600 hPa, right, respectively).

with RTTOV-9 and RTTOV-10, respectively.

The differences between RTTOV-10 and RTTOV-9 appear to be largest for infrared instruments, where upper stratospheric sounding channels are most affected. The differences are, however, generally small compared to the standard deviations of FG-departures or biases typically seen for these instruments. The largest effect can be seen for IASI channel 92 (Fig. 1), for which the standard deviations of the differences reach 0.2 K and RTTOV-10 produces brightness temperatures that are warmer by a few tenths of a Kelvin. For comparison, standard deviations of FG-departures for this channel are around 1.2 K; also, the channel is currently not used in the system due to the sensitivity to high levels. Interestingly, some of the tropospheric IR sounding channels still show small effects, for instance HIRS channel 5 (peaking around 600 hPa) shows differences of around 0.02 K (Fig. 2). This has been traced back to tails

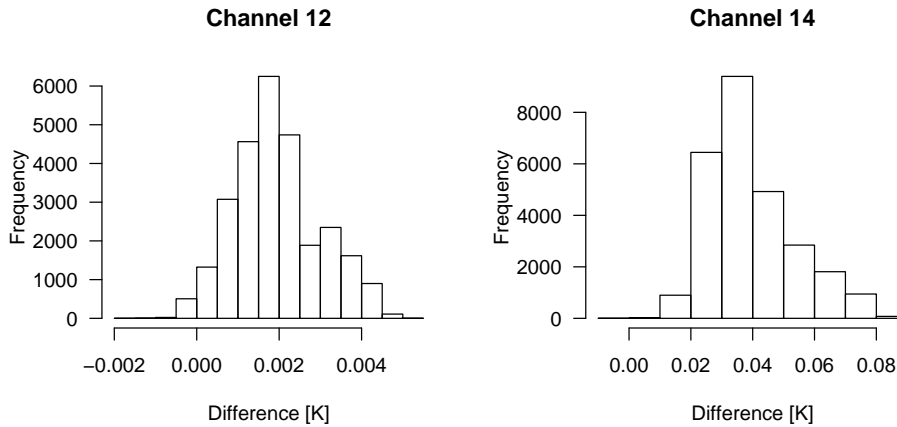


Figure 3: As Fig. 1, but for two AMSU-A channels (channel 12, peaking around 10 hPa, left, and channel 14, peaking around 2 hPa, right, respectively).

in the weighting functions in the upper stratosphere/mesosphere. The effect is again small compared to the standard deviation of FG-departures of just over 0.2 K for clear-sky data. For AMSU-A, the differences are largest for channel 14, but even for this channel they stay of the order of a few hundredth of a Kelvin, with RTTOV-10 producing slightly warmer brightness temperatures (Fig. 3). In comparison, standard deviations of FG departures for this channels are close to 1 K. For lower AMSU-A channels up to channel 10, and all other microwave instruments, the differences are negligible and generally less than around 0.001 K.

## 2.2 Analysis and forecast impact

To investigate the forecast impact of RTTOV-10 in the IFS, we ran several assimilation trials over extended periods. All were conducted using 4-dimensional variational assimilation with a 12-hour observation window, a model resolution of T511 ( $\approx 40$  km), an analysis resolution of T255 ( $\approx 80$  km) and 91 levels in the vertical. Two periods were run, covering two seasons: 1 July - 12 September 2010 and 1 January - 2 March 2011. The experiments used cycle 37r2 of the IFS, the system that became operational in May 2011. The Control experiment uses RTTOV-9, whereas the RTTOV-10 experiment uses RTTOV-10 as radiative transfer model. The RTTOV-10 experiment also includes a bugfix in the setting of azimuth angles for AMSU-A, a feature that was discovered during the course of the RTTOV-10 implementation. The bug has a very minor effect on the simulations of the ocean surface emissivity in RTTOV for some of the AMSU-A window channels used for quality-controlling the lower tropospheric channels. Both experiments assimilate the full observing system as operationally used with cycle 37r2.

As expected from the relatively small changes to the FG simulations noted above, the impact on the analyses is also rather small in the RTTOV-10 experiment. The minor changes to the biases in RTTOV are compensated for through minor adjustments in the variational bias correction, for instance for AMSU-A or HIRS (e.g., Fig. 4). After bias correction, FG departure statistics are not significantly altered, and also other observations do not indicate significant changes to the quality of the analyses.

Zonal mean temperature differences confirm that the impact of the different handling of the model top in RTTOV-10 is confined to the top-most model levels above 1 hPa. Here, no other observations currently

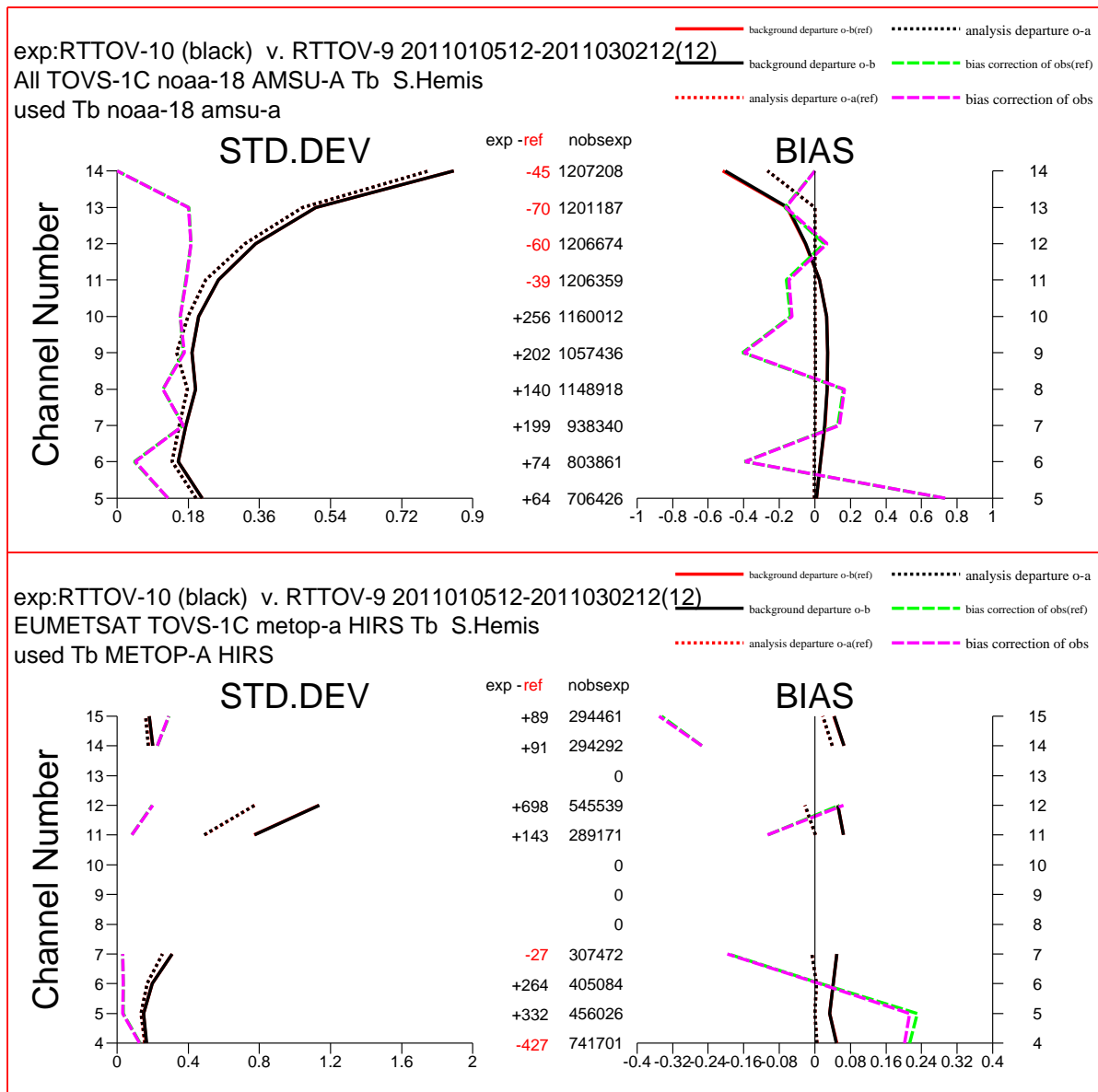


Figure 4: Departure statistics for NOAA-18 AMSU-A (top) and METOP-A HIRS (bottom) over the Southern Hemisphere for the period 5 January - 2 March 2011. Statistics for the RTTOV-10 experiment are shown in black, whereas statistics for the Control experiment are shown in red, with solid lines showing FG-departure statistics (observation minus FG) and dotted lines analysis departure statistics. Bias corrections are also shown, for the RTTOV-10 experiment in magenta and for the Control experiment in green. The number of observations for the RTTOV-10 experiment are given in the middle, including the difference between the RTTOV-10 and the Control experiment. The statistics are based on used observations.

provide information on the atmospheric state in the ECMWF system (Fig. 5), so they can be fairly sensitive to small changes in biases for radiances with some contribution from these levels. The differences are smaller than what has been encountered during the implementation of RTTOV-9 (Bormann et al. 2009), but nevertheless reach 10 K over the Southern Pole for the top-most model levels. Earlier comparisons with temperature retrievals suggest that over the polar regions such biases are not uncommon in the IFS

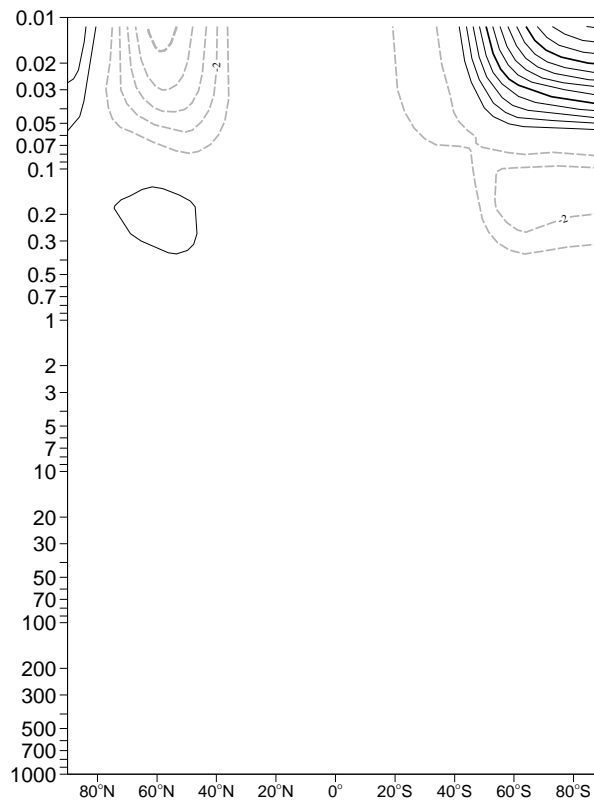


Figure 5: Zonal mean differences [K] for the temperature analyses between the RTTOV-10 and the Control experiment for January/February 2011. Positive values indicate that the RTTOV-10 experiment is warmer. Contour interval is 1 K and the zero-difference line is omitted.

system (Bormann et al. 2009).

The forecast impact of RTTOV-10 is neutral (not shown), consistent with the lack of significant changes to the tropospheric and lower stratospheric atmospheric analyses.

### 3 Impact of FASTEM-4

The fast microwave emissivity model (FASTEM) is used in RTTOV to model the ocean surface emissivity at microwave frequencies (e.g., Deblonde and English 2001). In cycle 37r2, FASTEM-3 is used for AMSU-A, -B, and MHS in the “clear-sky” route, whereas FASTEM-2 is used in the all-sky system for all other microwave sensors (except WINDSAT which is monitored passively and requires the use of FASTEM-3).

The ocean surface emissivity at microwave frequencies is affected by the permittivity of the water (primarily a function of salinity, temperature, and frequency), the roughness of the surface, and the presence of foam on the water (both related to surface wind and also a function of frequency). FASTEM-4 (Liu et al. 2011) employs a new permittivity parameterisation, based on fitting measurements for a wide frequency, temperature, and salinity range. As a result, salinity can now be provided as an input variable to FASTEM-4. For the roughness effects, regression coefficients for FASTEM-4 have been derived based on a new rigorous two-scale emissivity model and a full surface roughness spectrum model (a modi-

fied version of Durden and Vesecky 1985). Also the parameterisation describing the small-scale wave effects has been revised. In FASTEM-3, the regression coefficients for the large-scale part had been derived from a geometric optics model which has been shown to perform poorly for lower frequencies and also significantly underestimated the wind speed dependence for the horizontal polarisation. In addition, FASTEM-4 uses a new angular-dependent foam reflectivity parameterisation based on Kazumori et al. (2008), modelling the frequency-dependence following Stogryn (1972). The foam coverage follows the model of Tang (1974), replacing that of Monahan and O’Muircheartaigh (1986).

The use of FASTEM-4 has been investigated in the ECMWF system in assimilation experiments and compared to the previously used versions of FASTEM. The experimentation was done over the same periods and in the same setup as the Control and RTTOV-10 experiments described above. The only change compared to the RTTOV-10 experiment is that FASTEM-4 is used for all microwave sensors. Note that in the all-sky system the azimuthal dependence of the emissivities is neglected, primarily as it is not provided with the observations for some sensors. Additional experimentation with AMSR-E showed that the azimuthal dependence has a negligible effect on departure statistics (not shown). The experiment with RTTOV-10 and FASTEM-4 activated for all microwave instruments will be referred to as the FASTEM-4 experiment.

The FASTEM-4 experiment uses a constant salinity of 35 ‰, a representative value for ocean water. Ocean surface salinity, however, varies geographically, as shown in Fig. 6, typically between 25 ‰ for polar regions and to up to 40 ‰ over the tropics. To investigate the sensitivity of the radiative transfer computations to variations of the ocean surface salinity, additional tests have been performed in which the constant salinity value was set to 25 and 40 ‰, respectively. Fig. 7 shows that such changes typically lead to differences in the simulated brightness temperatures of a few tenths of a degree for the microwave imager channels used at ECMWF. The effect of ignoring the geographical variation of salinity is therefore relatively small for the frequencies considered in the atmospheric analysis, for which typical departures are of the order of Kelvins. Future developments could take geographical variations of salinity into account, and this may have an effect on the spatial variation of biases encountered against observations. Nevertheless, this is not seen as a priority for the currently assimilated frequencies.

In the following evaluation, we will ignore the first five days of each experiment in order to allow the variational bias correction to adjust to the new bias resulting from the changes in the radiative transfer model. An inspection of time series of the residual biases and the bias corrections shows that a 5 day period is sufficient in this case, as the bias changes are either small (as in the case of the RTTOV-10 experiment) or confined to surface-sensitive microwave observations.

### 3.1 Impact on departure statistics

In the following we summarise the impact on the departure statistics for the microwave instruments used in the assimilation experiments. Microwave instruments are treated in two different streams in the ECMWF system. The sounding instruments AMSU-A, -B, and MHS are assimilated in the “clear-sky” stream only in conditions diagnosed as clear. The imaging instruments/channels (AMSR-E, TMI, SSMI/S) are assimilated in the “all-sky” system in cloudy/rainy as well as clear conditions, primarily providing information on total column water vapour, rain and clouds in the ECMWF system.

The sounding and the imaging instruments employ different bias correction models in the variational bias correction. The sounding instruments use a linear model with a global constant and four layer thicknesses as airmass predictors. Scan-biases are modelled through a 3rd order polynomial in the scan position. The model is modified to exclude the airmass predictors for the window channels used for

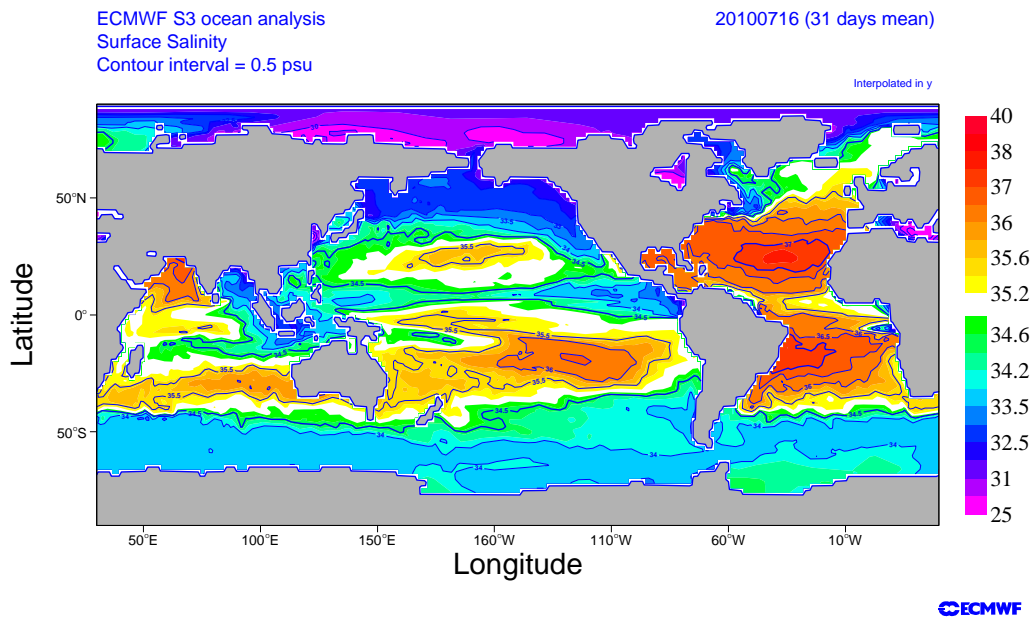


Figure 6: Surface salinity analysis for July 2010, taken from ECMWF's ocean reanalysis.

quality control, and to allow a different global offset and scan-bias over land for channels 4 and 5 of AMSU-A. In contrast, the imaging instruments/channels use a linear model with a global constant and the model's surface temperature, total column water vapour, and 10m wind speed as predictors. Scan-biases are again modelled through a polynomial in the scan position.

### 3.1.1 Microwave imagers

The microwave imager channels show the largest changes from using FASTEM-4, with significantly different bias corrections as a result of significantly different surface emissivity biases (Fig. 8). Using FASTEM-4 leads to, on average, warmer FG simulations, and the variational bias correction quickly adapts to this. It depends on the instrument whether the resulting mean bias corrections are smaller (indicating better agreement with the observations before bias correction) or not. For SSMIS, the mean bias corrections for the 19-37 GHz channels are generally reduced, demonstrating a better agreement with the observations before bias correction. For AMSR-E, similarly reduced bias corrections can be reported for the 19V and the 24 V and H channel (channels 5, 7, and 8), whereas the 19H and 37H channels (channels 6 and 10) now have bias corrections of similar or larger magnitude, but opposite sign. TMI similarly suggests a too strong warming for the 19H and 37H channels (channels 4 and 7), requiring larger absolute bias corrections than for FASTEM-2 for this instrument. The other TMI channels show similar or reduced bias corrections, and as for all three instruments the 22V channel (channel 5) still requires a considerable positive bias correction of 1 K or more. After bias correction, the changes in the mean biases of the FG or analysis departures are negligible, suggesting that the variational bias correction is similarly successful in removing the biases in both experiments.

The different relative biases in the simulations for the 37 GHz channels with FASTEM-4 have an important side-effect in the current assimilation of microwave imagers: they affect the estimate of cloudiness used in the observation error specification. The cloudiness parameter used in the observation error model is the difference between the vertically and horizontally polarised 37 GHz channels (Geer and Bauer

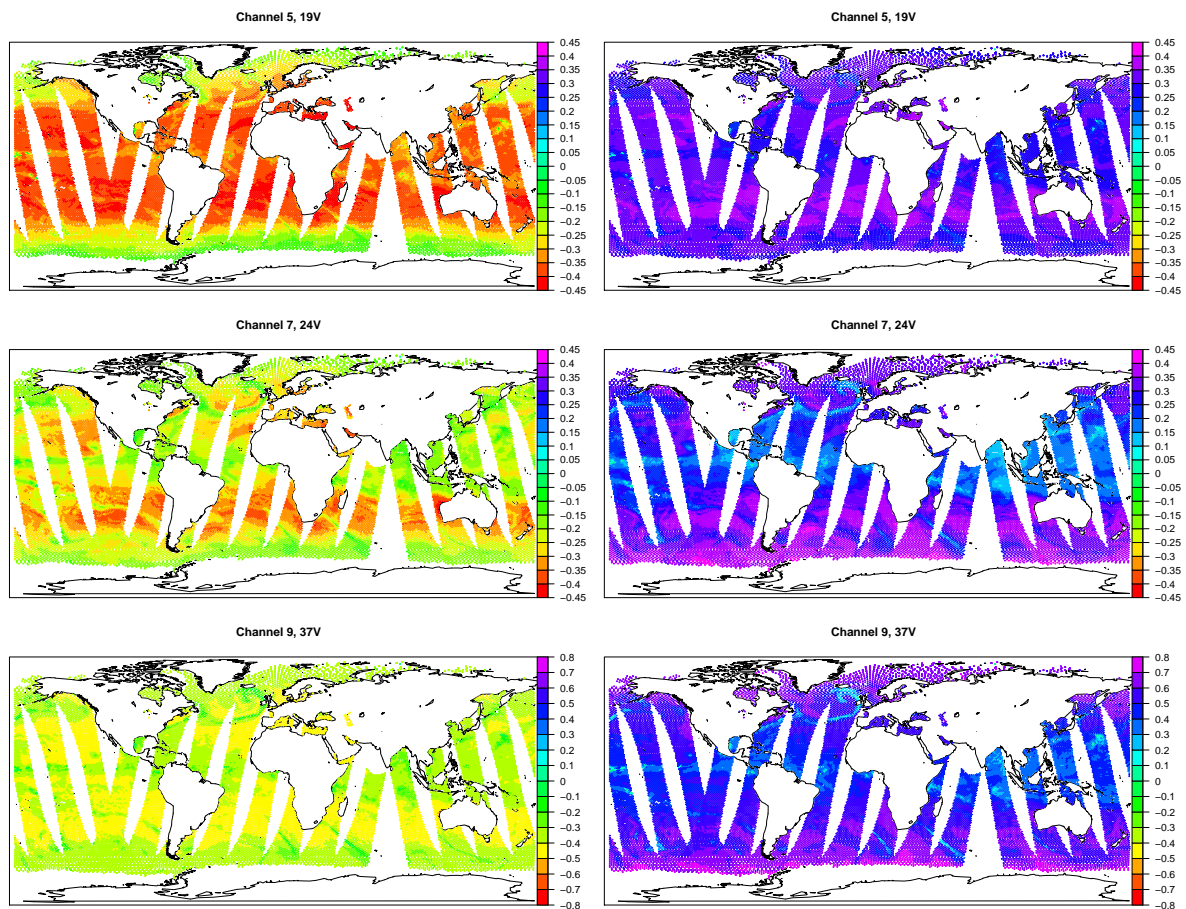


Figure 7: Impact of using different constant salinity values on FG simulations for selected AMSR-E channels, based on a 12-hour period covering 1 July 2010 0Z. The left panels show the difference between using a salinity of 25 ‰ vs 35 ‰, whereas the right panels show the difference between using a salinity of 40 ‰ and 35 ‰. The three channels are, from top to bottom, 5, 7, and 9.

2010), calculated as average from the observations and the FG simulations before bias correction. The differences in the biases act to reduce the estimate of cloudiness from the FG in the FASTEM-4 case and as a result reduce the observation errors for the microwave imager channels (by, on average 0.2-1.5 K, depending on the channel).

Standard deviations of FG departure statistics show encouraging signs in the FASTEM-4 experiment (Fig. 8). Standard deviations of bias corrections are significantly reduced for many channels, especially in the tropics, while the standard deviations of the FG departures after bias correction are mostly similar or slightly reduced compared to using FASTEM-2. The interpretation of this is not straightforward, as these statistics are affected by the increased weight given to the observations as a result of the implicit reduction of the observation errors. However, additional experimentation suggests that the reduction of the standard deviation of the bias corrections is a result of using FASTEM-4 regardless of the reduction of observation errors. This points to a better modelling of the spacial variability of surface emissivity in FASTEM-4. Exceptions are the 19H and 24H AMSR-E channels over the Southern Hemisphere which show larger standard deviations of bias corrections.

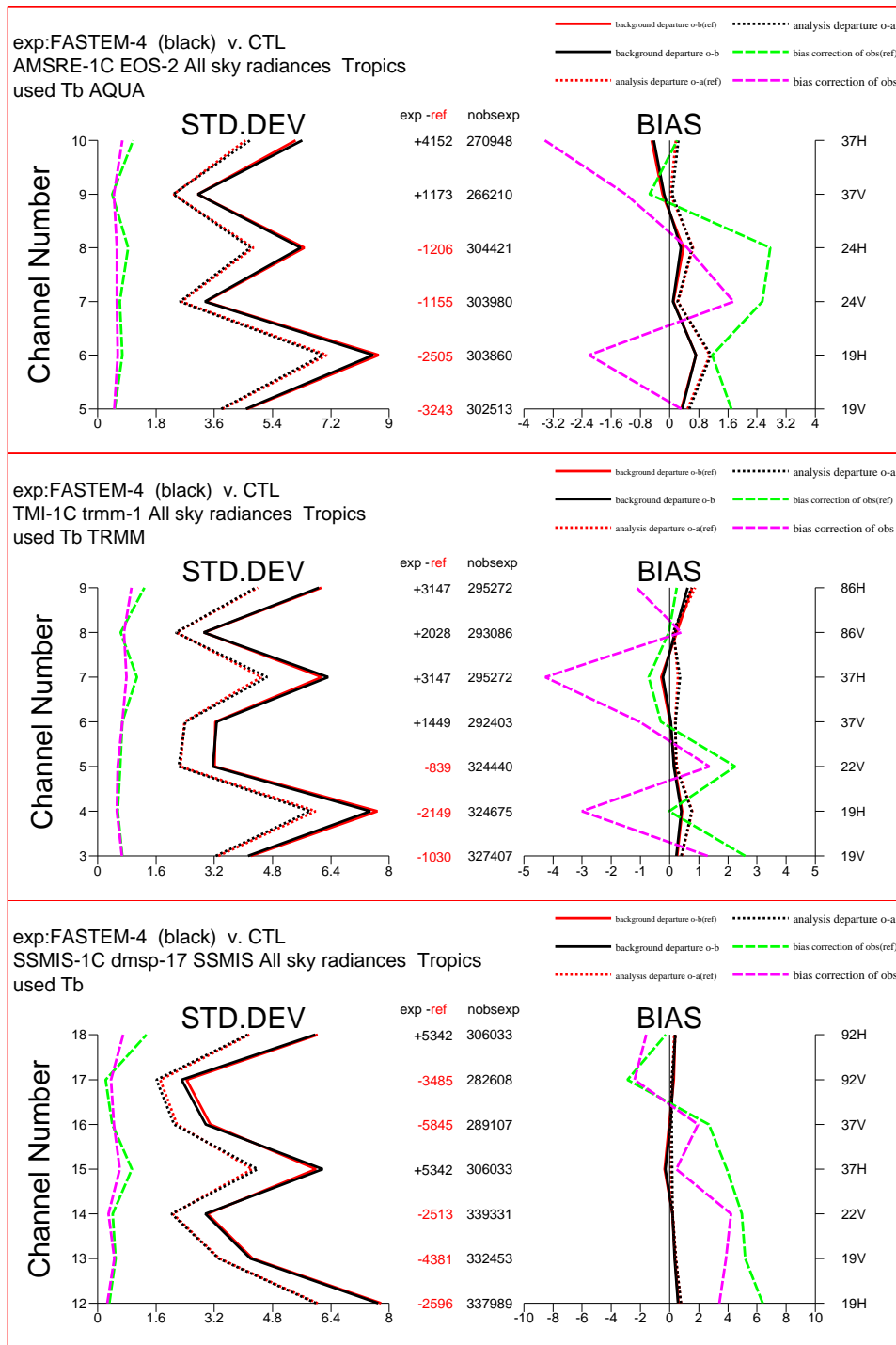


Figure 8: Departure statistics for microwave imager radiances over the tropics for the period 5-30 July 2010 for AMSR-E (top), TMI (middle), and SSMIS on F-17 (bottom). Statistics for the FASTEM-4 experiment are shown in black, whereas statistics for the Control experiment are shown in red, with solid lines showing FG-departure statistics (observation minus FG) and dotted lines analysis departure statistics. Bias corrections are also shown, for the FASTEM-4 experiment in magenta and for the Control experiment in green. The number of observations for the FASTEM-4 experiment are given in the middle, including the difference between the FASTEM-4 and the Control experiment. The statistics are based on used observations; note that some channels are shown as used here, but effectively carry no weight in the assimilation due to very large observation errors (channel 10 for AMSR-E, 7 and 9 for TMI, and 15 and 18 for SSMIS).

Closer inspection shows that FASTEM-4 leads to significantly different departure characteristics in regions of high surface wind speed, as highlighted in Fig. 9. The standard deviations of FG departures before bias correction show a notable reduction in regions of high 10m-wind speed for AMSR-E with FASTEM-4, which is considered a positive aspect as it suggests a reduction in the surface emissivity error in these regions. In terms of biases, the changes in bias for lower wind speed regions reflect the changes noted above in the bias correction, most likely related to the update of the roughness parameterisation. For 10 m-wind speeds exceeding about 15 m/s, FASTEM-4 gives increasingly larger emissivity values than FASTEM-2, leading to warmer FG values, reflected in increasingly larger changes in the bias. This aspect is most likely related to the change in the foam coverage model in FASTEM-4. The statistics show that the bias change addresses an underestimation apparent for FASTEM-2, yet for some AMSR-E channels the effect may now be overcompensated in FASTEM-4. However, note that the Figure displays the biases as a function of the 10 m wind speed of the FG, therefore inherently introducing a fast sampling bias for high wind speeds. Such a sampling bias would be consistent with a negative bias in terms of FG-departures. Qualitatively, this is what is observed in the statistics shown in Fig. 9, so the apparent remaining bias at high wind speeds for FASTEM-4 may merely reflect this sampling bias.

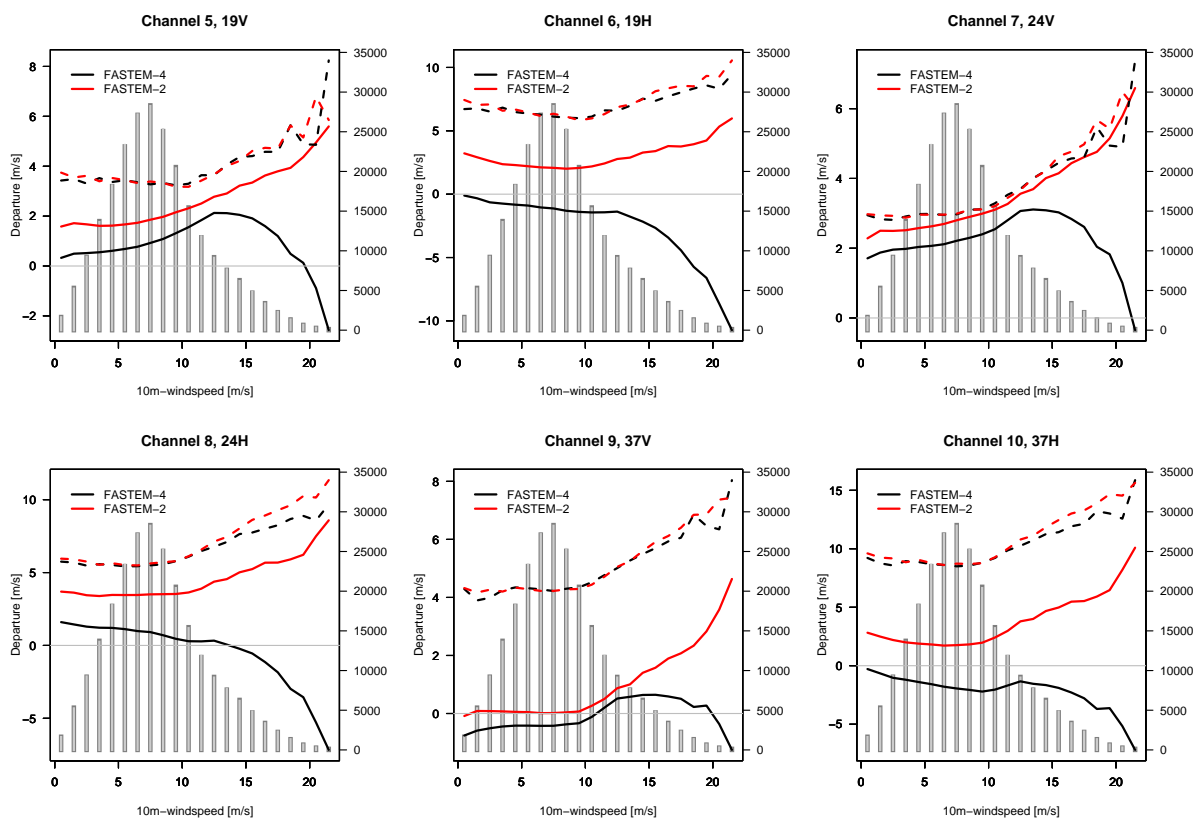


Figure 9: First Guess departure statistics before bias correction for the AMSR-E channels assimilated in the ECMWF system as a function of the model's 10m-wind speed, calculated for the period 5-25 July 2010 and based on all observations over sea. The statistics are derived from experiments that actively assimilated AMSR-E observations, using FASTEM-4 (black) or FASTEM-2 (red), respectively, with biases ( $Obs - FG$ ) displayed in solid lines, standard deviations with dashed lines. Also shown in grey is the population of data considered in the statistics as grey bars (right-hand x-axis).

Further analysis of the surface wind speed provided by the FG would be required to better attribute the bias to FASTEM-4, the FG wind speed, or the inherent sampling. Note that the 10m wind speed is one of the predictors in the variational bias correction, so some wind speed-dependent biases will be removed through the bias correction.

The wind speed dependence of the bias changes means that the changes to the assumed observation error for the microwave imager channels noted earlier is also dependent on the surface wind speed, with larger reductions in high wind speed regions, such as the high-latitude storm-tracks.

The reduction of the positive bias in high-windspeed regions observed for FASTEM-4 occurs in apparently similar locations to the "cold-sector" bias that we see with the microwave imagers: this is a long-standing phenomenon of large positive biases in cold, dry polar airmasses moving equatorward (Geer et al. 2009). Observations in these areas are excluded using tests based on modelled cloud and total-column water vapour amount (Geer and Bauer 2010). The most likely explanation for the "cold-sector" bias is insufficient modelled liquid water in mixed-phase Arctic stratocumulus clouds (e.g. Klein et al., 2009)

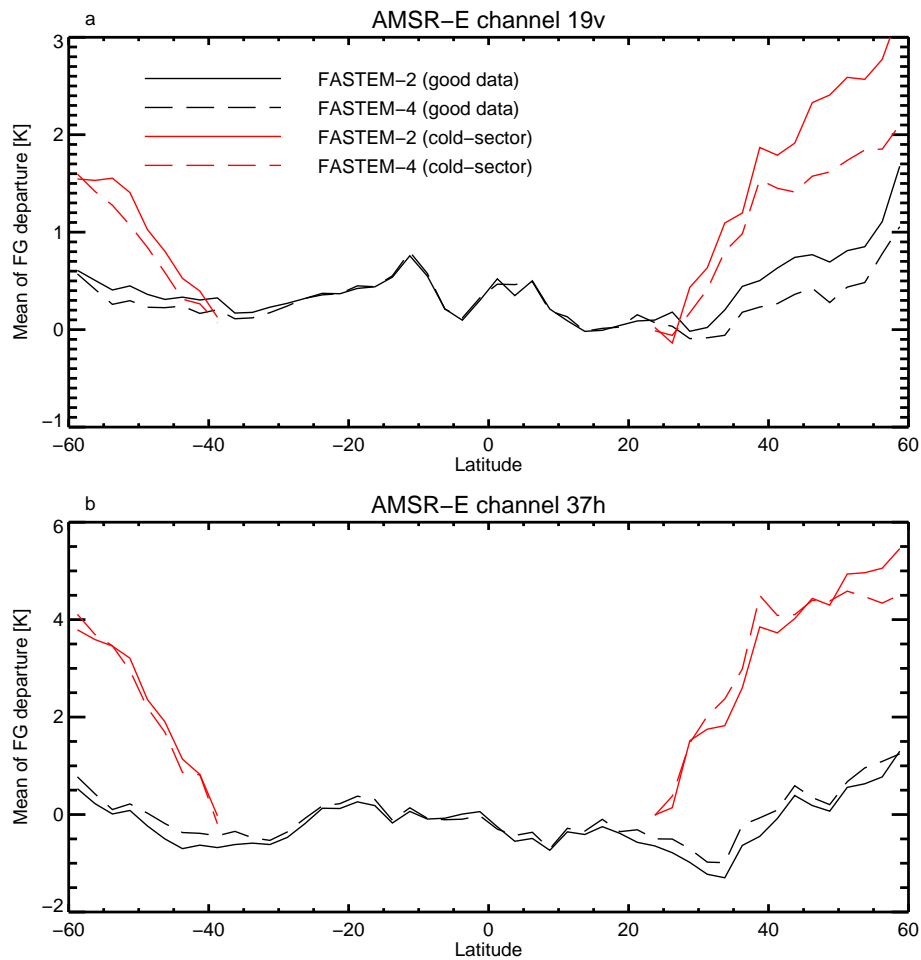


Figure 10: Zonal mean FG departures after bias correction for AMSR-E channels (a) 19V and (b) 37H, over the period 6 - 28 February 2011, using either FASTEM-2 or FASTEM-4. Two samples are shown: observations passing all-sky quality checks ("good", black lines) and those failing the cold-sector check but no others ("cold-sector", red lines).

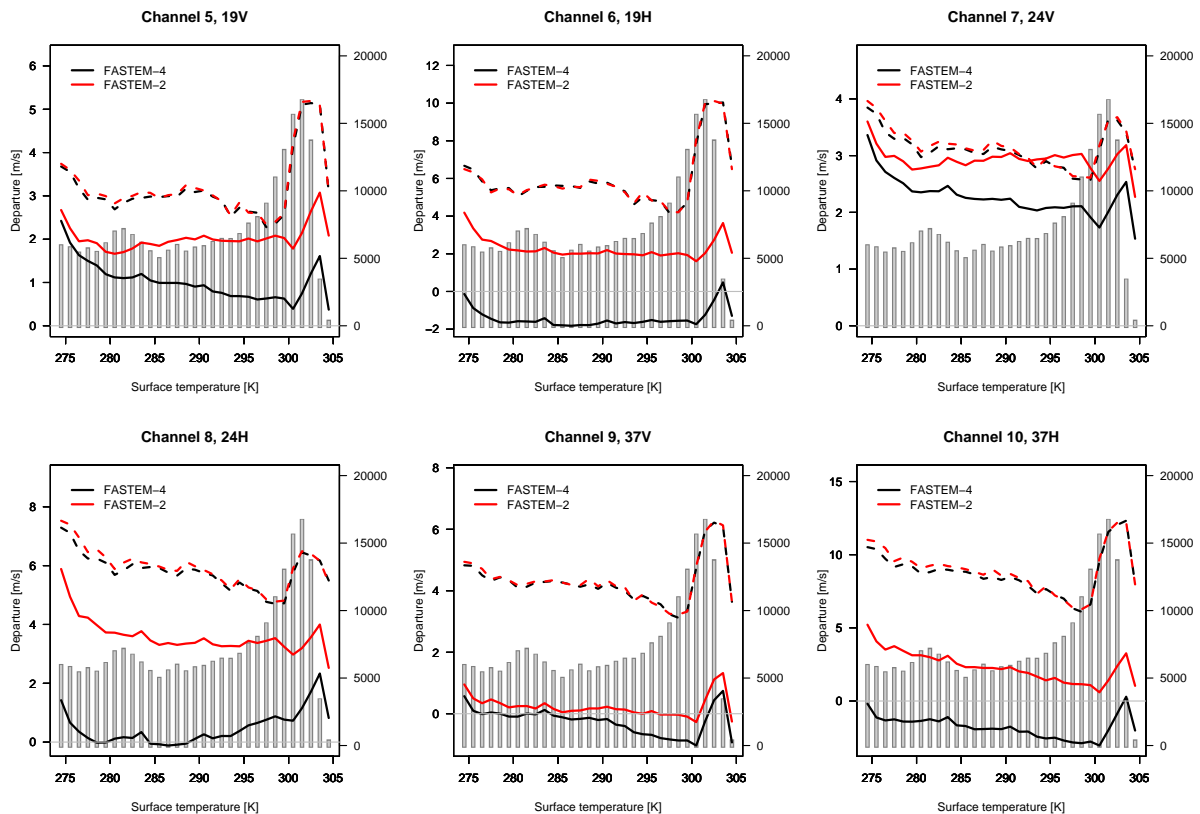


Figure 11: As Fig. 9, but for departure statistics as a function of surface temperature [K].

but we cannot yet rule out surface emissivity problems as an explanation. Hence, it is interesting to see if FASTEM-4 makes an improvement.

Figure 10 shows the effect of FASTEM-4 versus FASTEM-2 on zonal mean FG departures for AMSR-E. For a “good” sample, i.e. data which passes quality checks and is available for active assimilation, there are positive biases of up to 1 - 1.5 K at high latitudes, indicating that “cold-sector” screening is not perfect. Moving to FASTEM-4 reduces these biases by up to 0.4 K in channel 19V, but has very little effect on higher frequency channels such as 37H. For the sample of observations failing the “cold-sector” screening (but not including those failing any other quality check), there are much larger positive biases, up to 5.5 K in channel 37H, but the difference between FASTEM-4 and FASTEM-2 is similar to in the “good” sample. This suggests that the high-wind-speed regions are not much correlated with the “cold-sector” regions and that FASTEM-4 does not really address the cold-sector bias. That the “cold-sector” bias increases with frequency (and hence with sensitivity to cloud) might also suggest that it is a cloud rather than an emissivity problem.

FASTEM-4 also exhibits a different dependence on the surface temperature than FASTEM-2 for the vertically polarised channels, whereas the changes are largely independent of the surface temperature for horizontally polarised channels (Fig. 11). This aspect is particularly noticeable for channel 5 (19V) for which bias is fairly constant with surface temperature for FASTEM-2, whereas FASTEM-4 leads to an increasing bias with smaller surface temperatures. For high surface temperatures, Fig. 11 shows increased standard deviations of FG departures, most likely a result of forecast model problems in areas

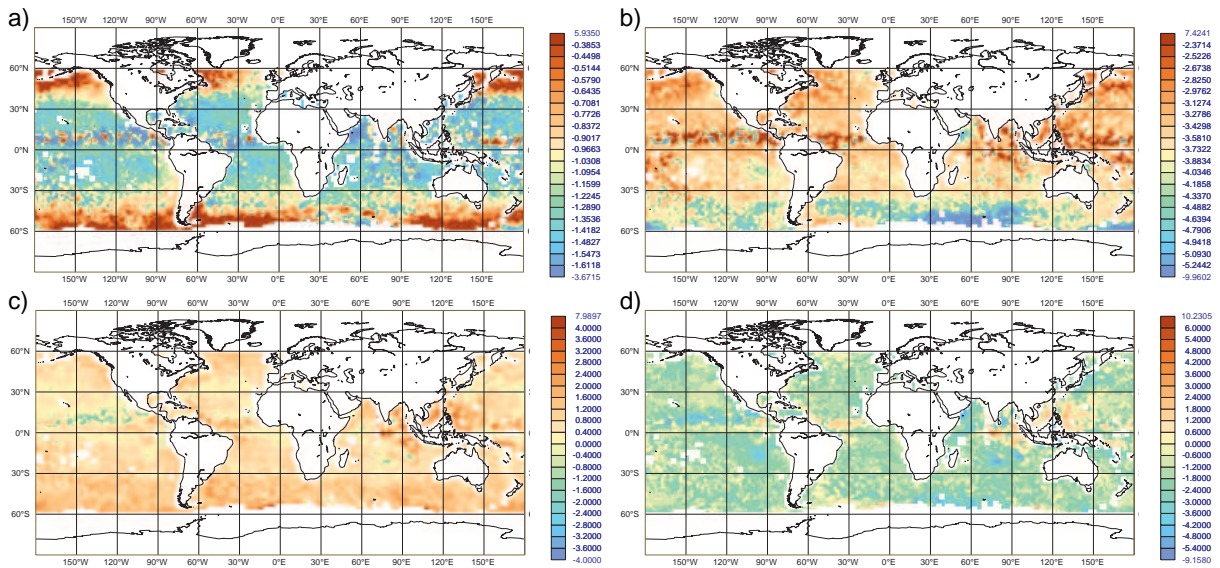


Figure 12: a) Difference in mean FG departures (obs-FG, K) before bias correction between the FASTEM-4 experiment and the Control for used data from channel 5 (19V) of AMSR-E over the period 5-31 July 2010. b) As a), but for channel 6 (19H). c) Mean FG departure (obs-FG, K) before bias correction for used data from channel 5 (19V) of AMSR-E over the period 5-31 July 2010 for the FASTEM-4 experiment. d) As c), but for channel 6.

of tropical deep convection; the feature is not present when cloudy conditions are excluded in the sample.

An example of the combined geographical effect of introducing FASTEM-4 is shown in Fig. 12. For channel 5, the zonal differences between FASTEM-4 and -2 expected from the surface temperature dependence of the biases are clearly visible, whereas for channel 6 the differences over the higher southern latitudes reflect the changes in the windspeed dependence of the bias characteristics.

### 3.1.2 Microwave sounders

The impact of the move to FASTEM-4 for AMSU-A is primarily confined to the window channels that are not assimilated, but used for quality control. This is highlighted in Fig. 13 showing the differences between clear-sky RTTOV-10 simulations with FASTEM-4 and FASTEM-3 as a function of 10m wind speed for selected viewing angles. The statistics show significantly different dependence on the 10m wind speed between the two emissivity models for the window channels (1-3 and 15), with differences of several Kelvin in high wind speed regions, and more modest changes of 1 or 2 K in low wind speed regions. The polarisations for AMSU-A channels changes with viewing angle, as does the sensitivity to the surface emissivity with the outer fields of view showing the smaller sensitivity. As a result, the differences in the bias characteristics between FASTEM-4 and FASTEM-3 reflect different characteristics for the vertical and the horizontal polarisations, as well as the influence of the different sensitivity to emissivity.

The changes in the biases arising from the use of FASTEM-4 are fairly modest compared to the biases between observations and FG-simulations typically experienced with FASTEM-3. Fig. 14 shows histograms of FG-departures before bias correction as a function of the 10m wind speed for the window channels of AMSU-A for simulations using FASTEM-4. Note that the FG simulations in this Figure neglect clouds, such that clouds in the observations appear as positive departures. The mode of the

histogram (ie the maximum of the distribution for a given wind speed) is expected to provide a more meaningful estimate of the bias. The Figure can be compared to the changes shown as a result of using FASTEM-4 instead of FASTEM-3 in Fig. 13. It can be seen that the four channels show biases of around 5 K for small zenith angles, and smaller positive biases for higher zenith angles. The warming of the FG as a result of using FASTEM-4 observed for all wind speeds for higher zenith angles in Fig. 14 appears beneficial, as this reduces a stronger positive bias otherwise present with FASTEM-3. In contrast, for small zenith angles, the cooling of the FG seen for wind speeds between 5 - 10 m/s as a result of using FASTEM-4 appears to have led to larger biases for many of the window channels. The bias with FASTEM-4 for channel 1 for low zenith angles is consistent with the bias observed for the 24V channel of AMSR-E, suggesting an underestimation of the emissivity. For low as well as higher zenith angles, high wind speeds continue to show positive departures for AMSU-A, a feature that is nevertheless improved in FASTEM-4 compared to FASTEM-3.

Over sea, a threshold on the absolute value of channel 3 departures is used in the ECMWF system to screen for too strong cloud/rain contamination. Overall, the mean bias of FG departures before bias

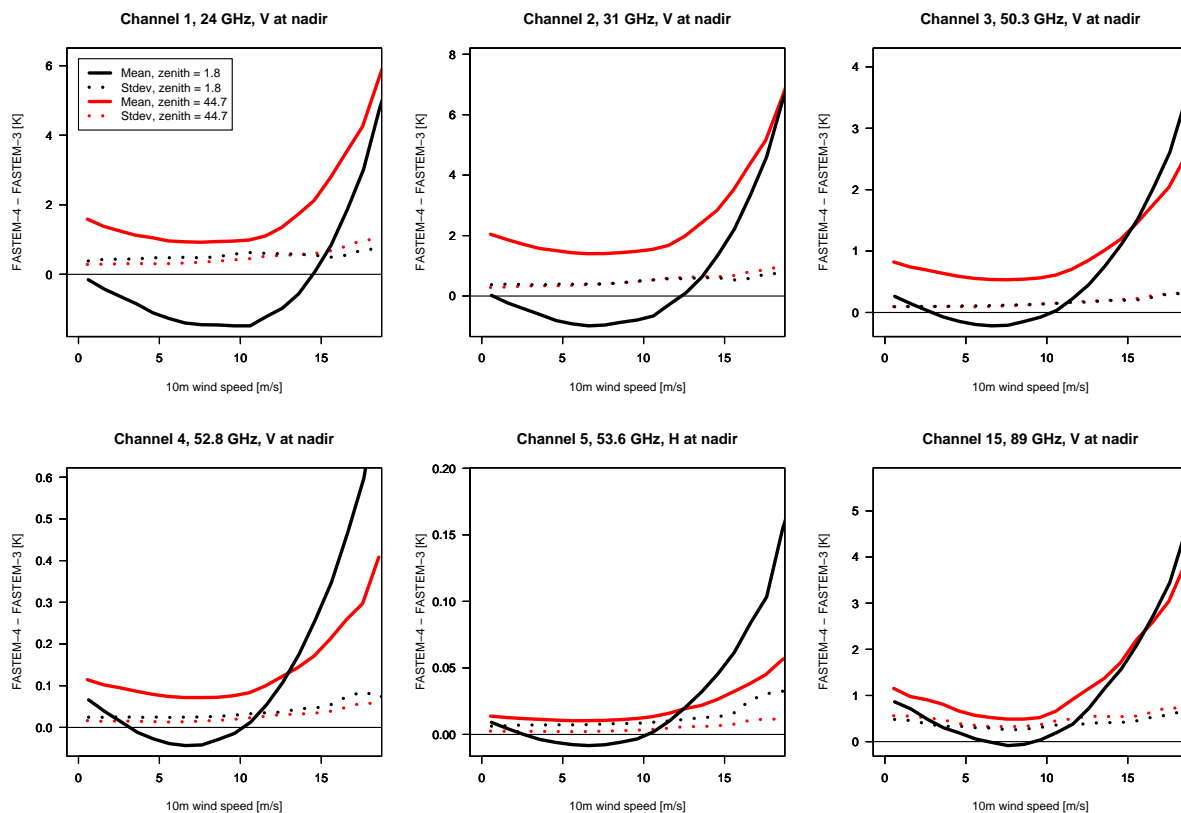


Figure 13: Differences between clear-sky brightness temperatures simulated with FASTEM-4 and with FASTEM-3 for AMSU-A channels with sufficient sensitivity to the surface. The statistics are shown in terms of the mean difference (solid line) and the standard deviation (dotted line) as a function of the 10m wind speed used in the simulations. Black lines give statistics for scan positions 15 and 16 (ie close to nadir), whereas red lines show statistics for scan positions 4 and 27 (zenith angle around  $44.7^\circ$ ). The latter are the outermost scan positions currently considered for assimilation. The statistics are based on over 25,000 simulations over sea, and the input data for the two simulations was the same.

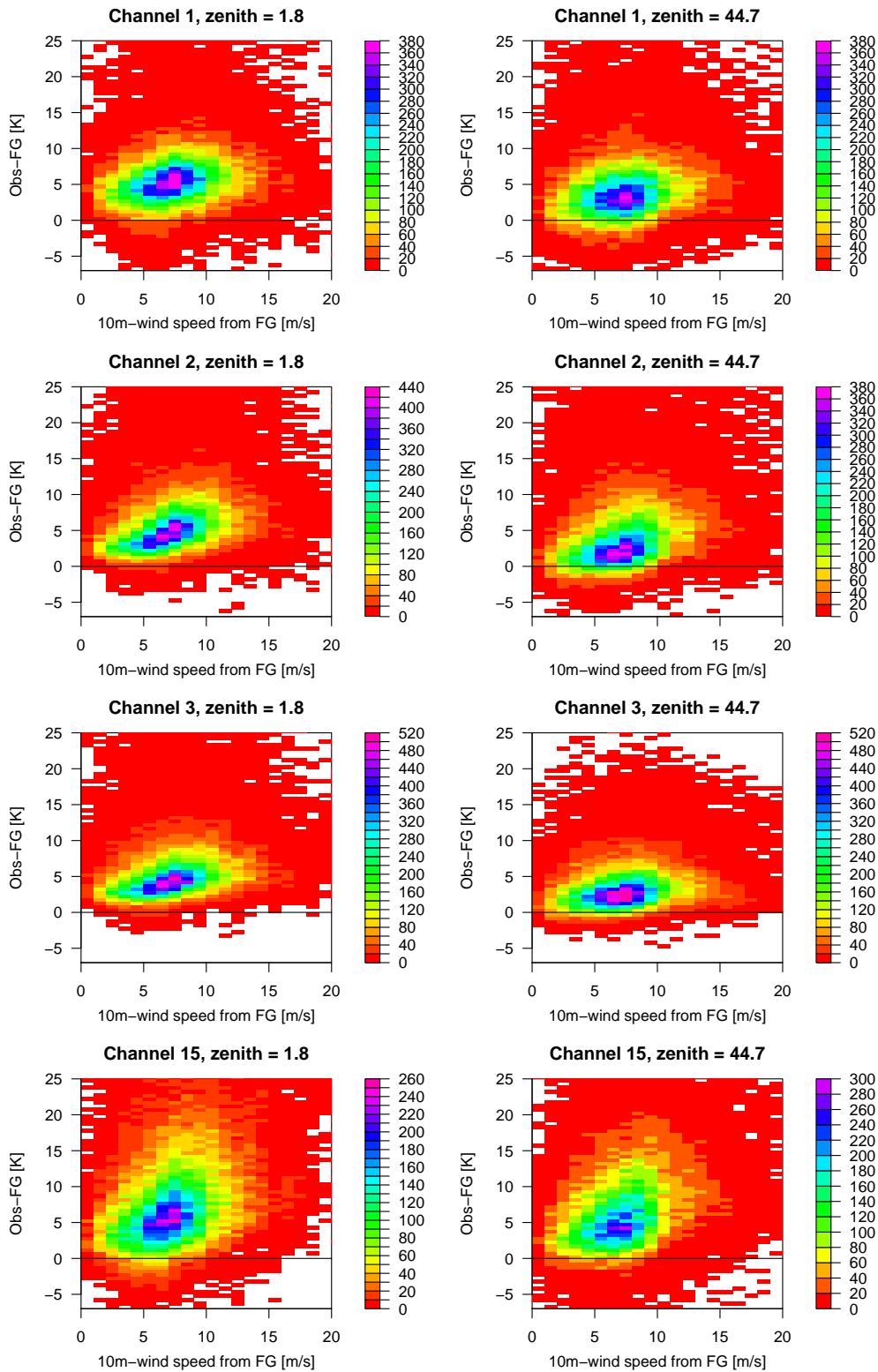


Figure 14: Two-dimensional histograms of the differences between observed and FG-simulated brightness temperatures before bias correction for the window channels of NOAA-18 AMSU-A as a function of the 10m-wind speed taken from the FG. The data is for the 3-day period 5-8 July 2010 from the FASTEM-4 experiment, over sea within  $\pm 60^\circ$  latitude, showing all data before quality control and thinning. The left column shows data for the central scan positions (zenith angle around  $1.8^\circ$ ), whereas the right column shows results for the outermost scan positions considered for assimilation at ECMWF (zenith angle around  $44.7^\circ$ ).

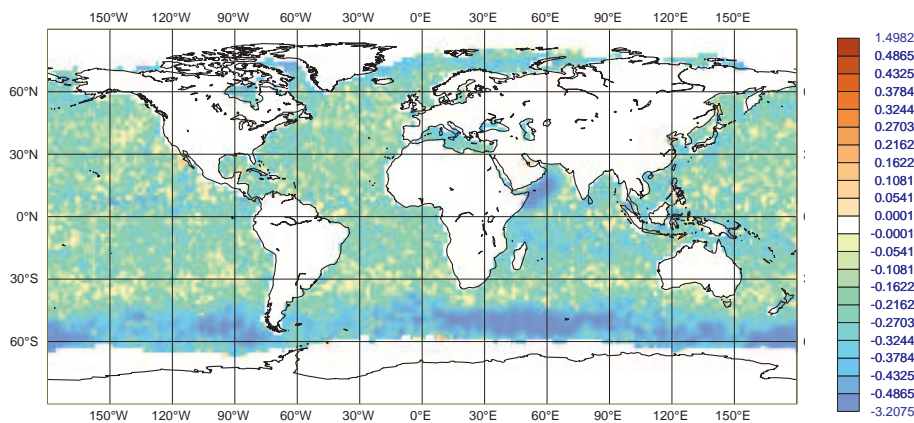


Figure 15: Difference in the mean FG departure before bias correction [K] between the FASTEM-4 and the Control experiment for METOP-A AMSU-A channel 3 after quality control, for the period 5-30 July 2010.

correction is typically reduced by a few tenth of a degree for this channel (Fig. 15), exceeding 0.5 K over the high surface wind speed regions of the Southern Hemisphere. The adjustments are largely absorbed by the bias correction for channel 3. However, the larger changes over the extra-tropical storm-tracks, combined with larger positive biases in these regions with FASTEM-3, lead to a slight increase in the number of used AMSU-A sounding observations in these regions (Fig. 16). The increase is around 2-3 % for the Southern Hemisphere for the July/August experiment. It is not clear whether this is a result of using more clear data that was previously erroneously flagged as cloudy/rainy, or because now more data with some cloud/rain-contamination is used. Mean FG departures before bias correction for channel 4 and screened in the same way as the lower-tropospheric sounding channels show a slight increase in the already positive biases over these regions, possibly an indication of additional cloud contamination (not shown). However, departure statistics for channel 5 and other lower tropospheric sounding channels show no significant change other than the increase in the number of used data (e.g., Fig. 17), so the increased numbers of used AMSU-A lower tropospheric sounding channels are not considered problematic.

For AMSU-B or MHS, the changes to the FG departure statistics are consistent with the findings for

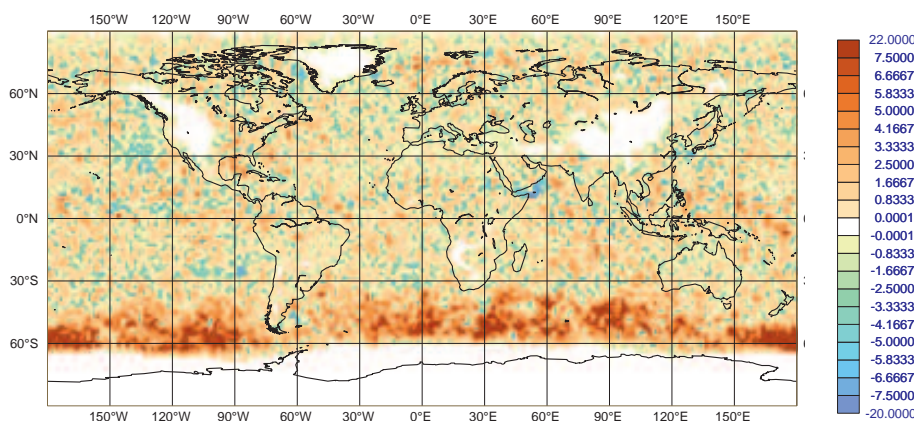


Figure 16: Difference in the number of used observations between the FASTEM-4 and the Control experiment for METOP-A AMSU-A channel 5, for the period 5-30 July 2010.

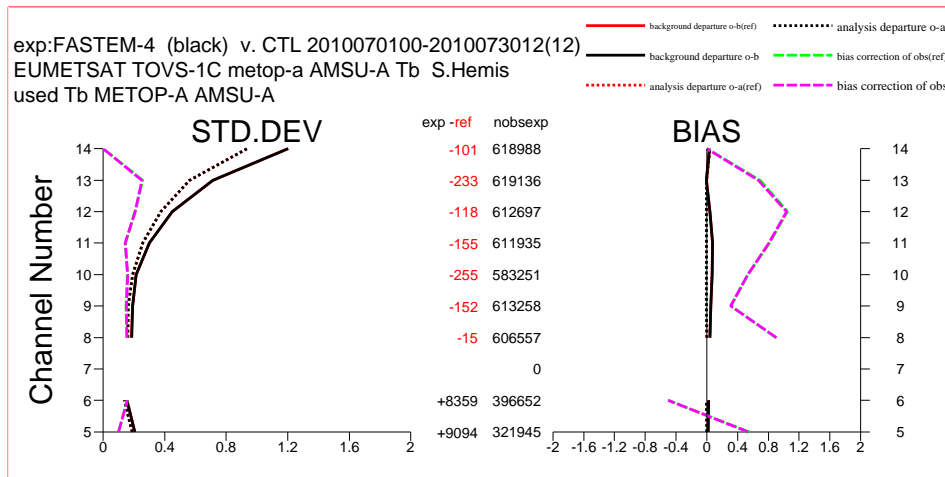


Figure 17: As Fig. 8, but for AMSU-A on METOP-A over the Southern Hemisphere.

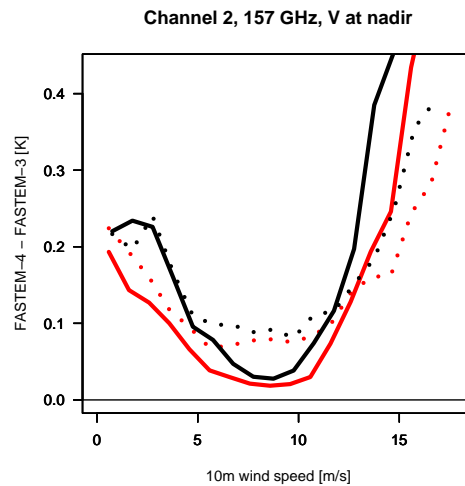


Figure 18: As Fig. 13, but for MHS channel 2.

AMSU-A. MHS channel 1 is similar to channel 15 of AMSU-A and shows the same characteristics (not shown). The change in the RTTOV simulations from FASTEM-3 to FASTEM-4 for MHS channel 2 is relatively small, staying below 0.5 K for most 10m-wind speeds (Fig. 18). Such changes are rather small compared to the standard deviations of FG departures observed for this channel (e.g., Fig. 19). Nevertheless, a check on the bias corrected FG departures for this channel is used to detect cloud/rain contamination for MHS, and the modified bias characteristics for high wind speeds lead to a very minor increase in the number of used observations (around 1 % over the Southern Hemisphere for the July/August experiment), similar to the one observed for AMSU-A (not shown). For other channels, the changes are negligible.

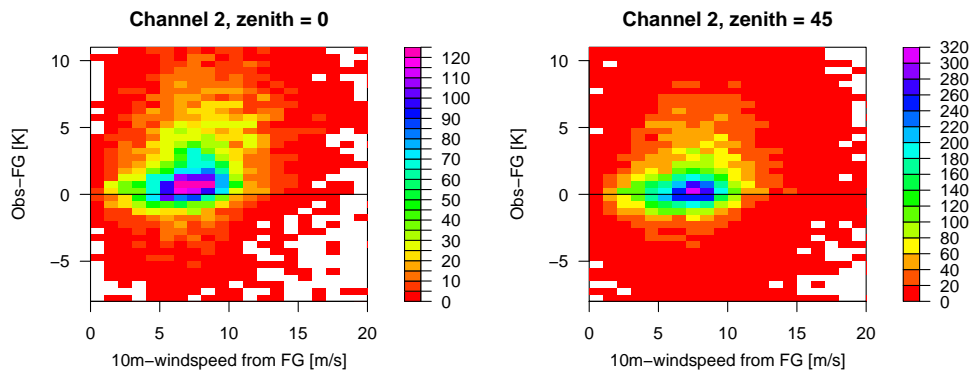


Figure 19: As Fig. 14, but for the METOP-A MHS channel 2. The left column shows data for the central scan position (zenith angle around  $0^\circ$ ), whereas the right column shows results for the outermost scan positions considered for assimilation at ECMWF (zenith angle around  $45^\circ$ ).

### 3.2 Analysis impact

In the following we will discuss only the combined impact of using RTTOV-10 and activating FASTEM-4, that is, we compare the FASTEM-4 experiment with the Control.

For radiance observations, the modifications to the observation departure statistics are a combination of the effects described earlier, that is, changes to the bias corrections for the channels with some sensitivity to the top-most model levels (e.g., Fig. 4), changes to the bias corrections for the surface-sensitive microwave radiances, esp. the imagers (e.g., Fig. 8), and a slight increase of the use of AMSU-A data over regions of high near-surface wind speeds (e.g., Fig. 16). Otherwise, the fit is not significantly altered, supporting the overall consistency of the changes introduced through RTTOV-10 and FASTEM-4.

Departure statistics for non-radiance observations are not significantly altered in the FASTEM-4 experiment compared to the Control (not shown), suggesting that both experiments agree similarly well with the rest of the observing network.

Changes to the mean analyses are also small for the troposphere, with changes to the mean analysis of geopotential usually less than 1 gpm, of temperature less than 0.1 K, and of relative humidity less than 2 %. In the stratosphere, the modifications to the handling of the top of the atmosphere in RTTOV-10 lead to changes in the mean analysis as shown earlier in Fig. 5.

### 3.3 Forecast impact

The forecast impact of RTTOV-10 with FASTEM-4 is overall neutral when verified against analyses or observations (e.g., Figures 21 and 20). This is consistent with the small changes in the departure statistics after bias corrections for radiances and other observations pointed out earlier.

An apparent degradation is notable in the short-range around  $60^\circ$  South for the lower troposphere for both seasons (e.g., Fig. 20). This feature is present for all variables and particularly noticeable for humidity. The feature is a result of the implicit reduction of the observation error for the microwave imagers mentioned earlier, leading to an increase in weight for this data in the analysis, especially in the high wind-speed regions of the Southern Hemisphere storm-tracks. This results in increased variability of the analyses, appearing as increased root mean square errors (RMSE) of the short-range forecasts in

RMS forecast errors in Z(fi52-fhqv), 5-Jul-2010 to 12-Sep-2010, from 62 to 70 samples.

Point confidence 99.5% to give multiple-comparison adjusted confidence 90%. Verified against own-analysis.

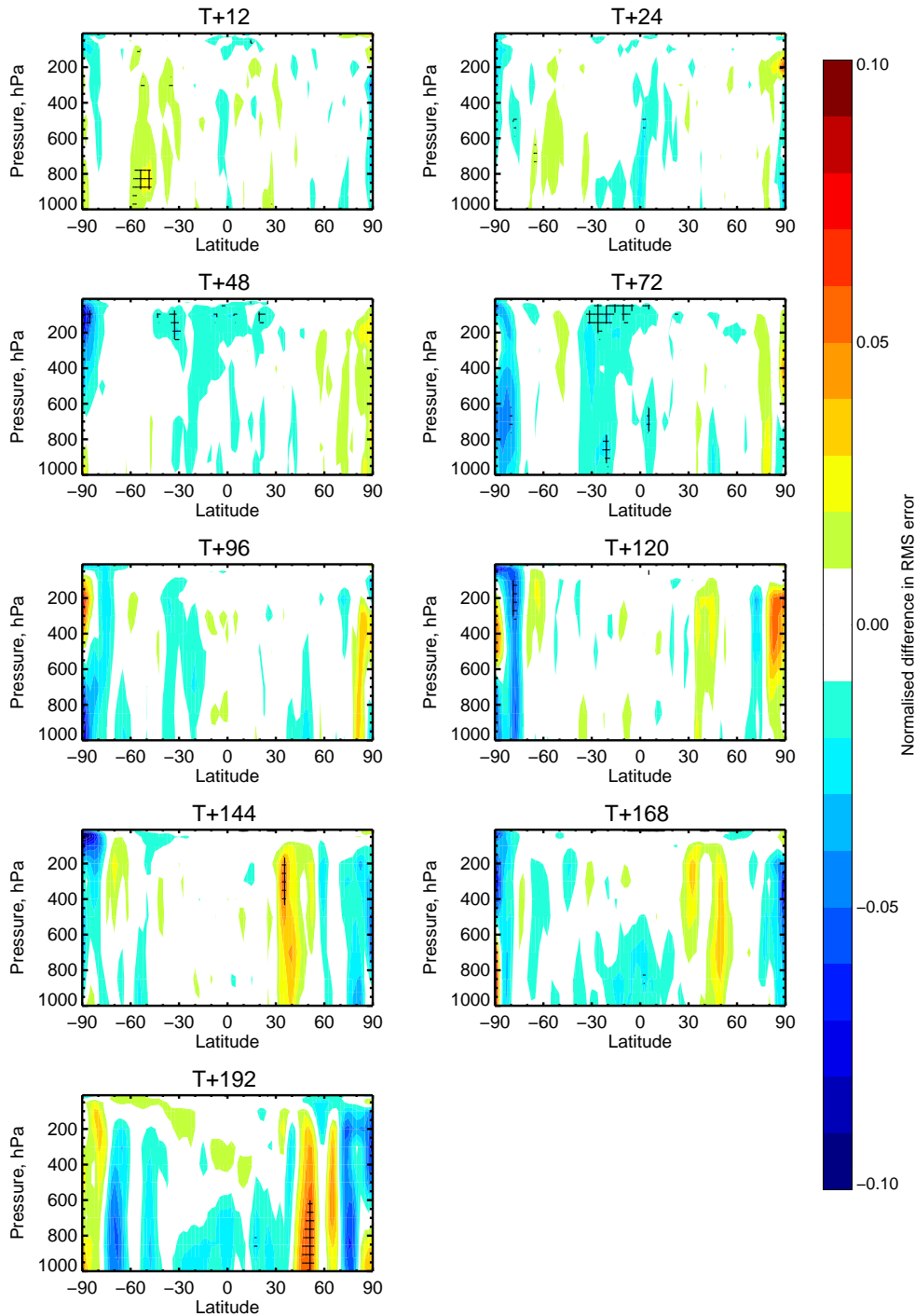


Figure 20: Zonal means of the normalised difference in the root mean squared forecast error of the geopotential between the FASTEM-4 experiment and the Control for the July/September experiment. Positive values indicate an increase in the RMSE, and hence a degradation from using RTTOV-10 with FASTEM-4. Verification is against the own analysis, and hatching indicates regions of statistically significant changes. The nine panels show results for different forecast lead times, as indicated above each panel.

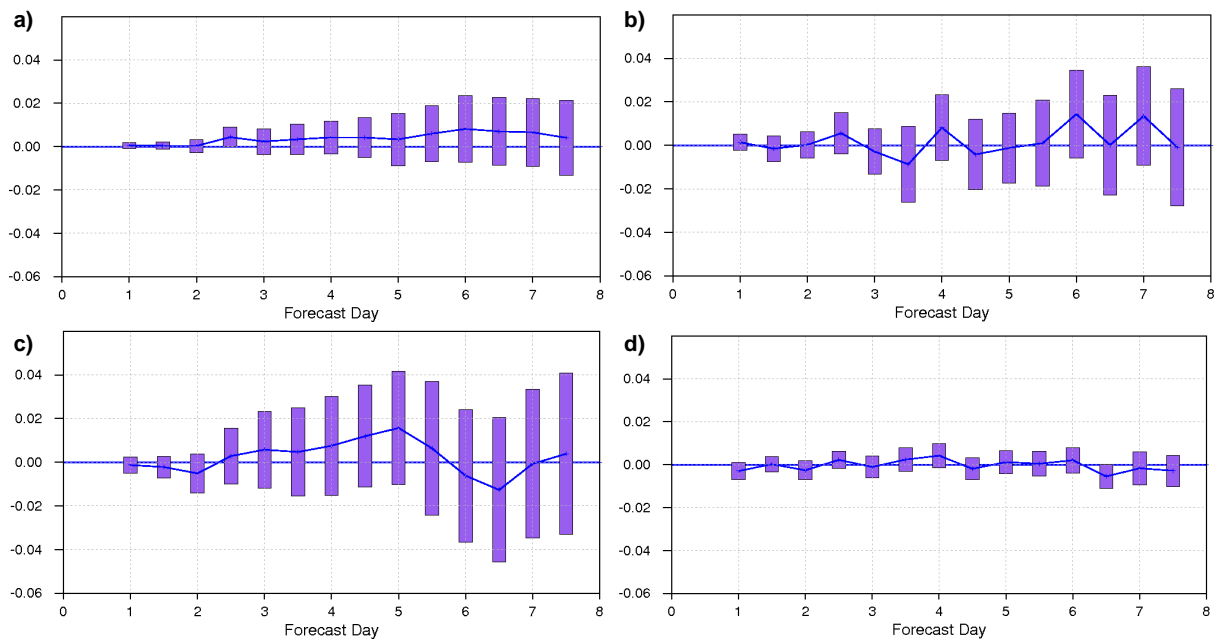


Figure 21: a) Normalised difference in the root mean square error (RMSE) of the 500 hPa geopotential between the FASTEM-4 and the Control experiment for the Northern Hemisphere as verified against radiosonde observations. Results for both periods are pooled together (127 cases). Error bars indicate 95% confidence intervals. b) As a), but for the Southern Hemisphere. c) As a), but for Europe. d) As a), but for the 850 hPa wind forecast over the tropics.

verifications against the own analysis. The feature is not accompanied with a significant degradation of the FG-fit to other observations, and also does not lead to an increase in the RMSE for longer forecast ranges, so the feature is not considered problematic. Nevertheless, an additional experiment has been run for the July/September period in which the parameters of the observation error model for the microwave imagers were adjusted in order to counteract the observation error reduction otherwise present in the FASTEM-4 experiment. With the adjusted parameters the noted apparent degradation is substantially reduced, whereas the forecast impact remains otherwise neutral (not shown).

## 4 Conclusions

This memorandum documents the effects of using RTTOV-10 in the ECMWF system. The main changes are a modification to the handling of the top of the atmosphere in RTTOV-10, and the use of FASTEM-4 as emissivity model. The main findings are:

- FASTEM-4 significantly alters the bias characteristics seen in departure statistics for surface-sensitive microwave sensors over sea, especially for the imager channels. For some sensors this means smaller bias corrections are required, whereas for others the absolute value of the bias corrections increase for some channels. Over all sensors considered, it appears that FASTEM-4 brings mean biases to within inter-satellite biases for the surface-sensitive microwave channels considered in this study. Exceptions are the 22/24 and 50.4 GHz vertically polarised observations for which FASTEM-4 still appears to significantly underestimate the surface emissivity. As a result, the benefits of FASTEM-4 for AMSU-A simulations over FASTEM-3 are less clear.

- FASTEM-4 shows very different bias characteristics as a function of 10m wind speed compared to FASTEM-2 or FASTEM-3. The different characteristics appear overall to be an improvement when compared to radiance observations, even though for some channels the 10m wind speed dependence may be overestimated.
- The larger bias changes for high surface wind speeds lead to an increased number of tropospheric AMSU-A observations allowed in the analysis in these regions as a result of quality control practices used at ECMWF.
- The change in the relative biases for the 37 GHz channels of the microwave imagers leads to a reduction of the observation errors for these observations, an artifact of the observation error model used for these observations. The effect is largest in regions of high 10m wind speeds, as the relative bias differences are largest here.
- The modifications introduced for the treatment of the top-of-the-atmosphere with RTTOV-10 lead to minor changes to the departure characteristics of channels with some sensitivity to the top of the atmospheric model. Nevertheless, changes are noticeable in the mean temperature analyses above 1 hPa.

Given the overall improvement in terms of the bias characteristics for the microwave imager channels and the otherwise neutral performance, RTTOV-10 with FASTEM-4 has been included in cycle 37r3 of the IFS configuration.

Subsequent to the official release of RTTOV-10, revisions to FASTEM-4 have been developed by Q. Liu and others, and an updated version, to be referred to as FASTEM-5, is now being investigated. The developments have been prompted by the somewhat disappointing performance of FASTEM-4 for some of the AMSU-A channels, and by indications that the change in the wind speed-dependence of the bias characteristics is too large. The presented evaluation will have to be repeated with this new version. It is expected that the variational bias corrections will also be able to neutralise the undoubtedly changed bias characteristics.

## Acknowledgements

Help from James Hocking (Met Office) in debugging early versions of RTTOV-10 is gratefully acknowledged, as is assistance from Deborah Salmond and John Hague regarding the computational performance evaluation of RTTOV-10. RTTOV is developed by the NWP SAF, with joint contributions from ECMWF, Météo France, and the UK Met Office.

## References

- Bormann, N., D. Salmond, M. Matricardi, A. Geer, and M. Hamrud, 2009: The RTTOV-9 upgrade for clear-sky radiance assimilation in the IFS. Technical Memorandum 586, ECMWF, Reading, UK, 26 pp [available under [www.ecmwf.int/publications/library/do/references/list/14](http://www.ecmwf.int/publications/library/do/references/list/14)].
- Deblonde, G., and S. English, 2001: Evaluation of the fastem-2 fast microwave oceanic surface emissivity model. In Tech. Proc. ITSC-XI Budapest, 67–78.
- Durden, S., and J. Vesecky, 1985: A physical radar cross-section model for a wind-driven sea with swell. *IEEE J. Oceanic Eng.*, **OE-10**, 445–451.

- Geer, A., and P. Bauer, 2010: Enhanced use of all-sky microwave observations sensitive to water vapour, cloud and precipitation. Technical Memorandum 620, ECMWF, Reading, UK, 41 pp [available under [www.ecmwf.int/publications/library/ecpublications/\\_pdf/tm/601-700/tm620.pdf](http://www.ecmwf.int/publications/library/ecpublications/_pdf/tm/601-700/tm620.pdf)].
- Geer, A., P. Bauer, and C. O'Dell, 2009: A revised cloud overlap scheme for fast radiative transfer in rain and cloud. *J. Appl. Meteor.*, **48**, 2257–2270.
- Han, Y., 2007: Incorporation of the JCSDA Zeeman RT model in RTTOV v9. Nwp saf report, Met.Office, 30pp.
- Kazumori, M., Q. Liu, R. Treadon, and J. Derber, 2008: Impact study of AMSR-E radiances in the NCEP global data assimilation system. *Mon. Wea. Rev.*, **136**, 541–559.
- Klein, S., R. McCoy, H. M. A. A. AS, A. Avramov, G. Boer, M. Chen, J. Cole, A. Del Genio, M. Falk, M. Foster, A. Fridlind, J. Golaz, T. Hashino, J. Harrington, C. Hoose, M. Khairoutdinov, V. Larson, X. Liu, Y. Luo, G. McFarquhar, S. Menon, R. Neggers, S. Park, M. Poellot, J. Schmidt, I. Sednev, B. Shipway, M. Shupe, D. Spangenberg, Y. Sud, D. Turner, D. Veron, K. Salzen, G. Walker, Z. Wang, A. Wolf, S. Xie, K. Xu, F. Yang, and G. Zhang, 2009: Intercomparison of model simulations of mixed-phase clouds observed during the ARM Mixed-Phase Arctic Cloud Experiment. I: single-layer cloud. *Q. J. R. Meteorol. Soc.*, **135**, 979–1002.
- Liu, Q., F. Weng, and S. English, 2011: An improved fast microwave water emissivity model. *IEEE Trans. Geosci. Remote Sens.*, **49**, 1238–1250.
- Matricardi, M., 2010: A principal component based version of the RTTOV fast radiative transfer model. *Q. J. R. Meteorol. Soc.*, **136**, 1823–1835.
- Monahan, E., and I. O'Muircheartaigh, 1986: Whitecap and the passive remote sensing of the ocean surface. *Int. J. Remote Sensing*, **7**, 627–642.
- Rochon, Y., L. Garand, D. Turner, and S. Polavarapu, 2007: Jacobian mapping between vertical coordinate systems in data assimilation. *Q. J. R. Meteorol. Soc.*, **133**, 1547–1558.
- Saunders, R., M. Matricardi, and P. Brunel, 1999: An improved fast radiative transfer model for assimilation of satellite radiance observations. *Q. J. R. Meteorol. Soc.*, **125**, 1407–1426.
- Stogryn, A., 1972: The emissivity of sea foam at microwave frequencies. *J. Geophys. Res.*, **77**, 1658–1666.
- Tang, C., 1974: The effect of droplets in the air-sea transition zone on the sea brightness temperature. *J. Phys. Oceanography*, **4**, 579–593.